RESEARCH PAPER

PCCP
www.rsc.org/pccp

The photochemical production of HONO during the heterogeneous hydrolysis of NO_2

Kevin A. Ramazan, Dennis Syomin and Barbara J. Finlayson-Pitts*

Department of Chemistry, University of California, Irvine CA 92697-2025, USA. E-mail: bjfinlay@uci.edu; Fax: +1 (949) 824-3168; Tel: +1 (949) 824-7670

Received 12th February 2004, Accepted 12th May 2004
First published as an Advance Article on the web 1st June 2004

The heterogeneous hydrolysis of NO_2 in thin water films, a major source of HONO and hence OH radicals in polluted urban atmospheres, has been previously reported to be photoenhanced (H. Akimoto, H. Takagi and F. Sakamaki, *Int. J. Chem. Kinet.*, 1987, **19**, 539, ref. 1) which has important implications for OH production both in environmental chambers and in the lower atmosphere. We report here studies of the impact of 320–400 nm radiation on HONO formation during the heterogeneous NO_2 hydrolysis at 296 K. The experiments were carried out in a borosilicate glass cell using long path Fourier transform infrared (FTIR) spectroscopy with three initial NO_2 concentrations (20, 46, and 54 ppm) at relative humidities of 33, 39, and 57%, respectively. Nitrous acid was first allowed to accumulate from NO_2 hydrolysis in the dark, and then the mixture of reactants and products was irradiated. The measured concentration–time profiles of the gases were compared to the predictions of a kinetics model developed for this system. The initial loss of HONO upon irradiation was consistent with its photolysis and known secondary gas phase chemistry without any photoenhancement. While the fundamental NO_2 heterogeneous hydrolysis is not itself photoenhanced, there is clear evidence in these experiments for the generation of gas phase HONO by photolysis of adsorbed HNO_3 formed during the heterogeneous hydrolysis. The mechanisms and atmospheric implications of HONO as well as NO_2 formation by the photolysis of surface-adsorbed HNO_3 are discussed.

Introduction

Nitrous acid (HONO) was first identified spectroscopically in ambient urban air in 1979.[2] Since then, a number of atmospheric measurements have shown that HONO accumulates during the night and undergoes photolysis in the early morning to produce a pulse of hydroxyl radicals (OH).[3–10] Indeed, HONO photolysis is the major source of OH in the early morning in high NO_x locations, and is a significant source even when averaged over 24 h.[4,6,9,10] Since OH drives the chemistry that leads to the formation of O_3 and a variety of other secondary air pollutants,[11] it is important to understand the sources and sinks of HONO and the mechanism of its formation.

The major atmospheric source of HONO is believed to be the heterogeneous hydrolysis of NO_2, generally represented by

$$2NO_2 + H_2O \xrightarrow{\text{surface}} HONO + HNO_3 \qquad (1)$$

The surfaces available for reaction include airborne particles, soils, and urban surfaces such as glass, concrete and foliage.[5–7,12] Although reaction (1) has been the subject of a number of laboratory studies,[1,12–29] the mechanism of this reaction has been difficult to elucidate. This laboratory has recently proposed a mechanism for reaction (1) in which dinitrogen tetroxide (N_2O_4) is a key intermediate.[12] A schematic diagram of that mechanism, updated to reflect recent findings,[30,31] is shown in Fig. 1.

In this mechanism, gaseous N_2O_4, in equilibrium with NO_2, is taken up into the water film present on the surface. There, the N_2O_4 isomerizes to asymmetric $ONONO_2$, which autoionizes to form $NO^+NO_3^-$ at the surface. This ion pair reacts with surface film water to form adsorbed HONO and HNO_3. The HNO_3 remains on the surface while HONO is either displaced into the gas phase by the competitive adsorption between water and HONO,[30] or undergoes secondary chemistry to produce gaseous NO, NO_2, and small amounts of N_2O. In order for HONO production to be first order in NO_2, as many previous studies reported,[12,17–26] a back reaction involving NO_2 reacting with $ONONO_2$ must be faster than the competing reaction with water.

A photoenhancement of the generation of HONO from the heterogeneous hydrolysis of NO_2 was reported by Akimoto *et al.*[1] The HONO formed in a 6065-L PFA Teflon (tetrafluoroethylene-perfluoroalkyl vinyl ether copolymer) coated smog chamber did not decay as rapidly as predicted by a model of the chemistry when the mixture in air was irradiated with a filtered Xe lamp ($\lambda > 290$ nm). The difference between the model-predicted and experimental data was attributed to a photoenhancement of the kinetics of HONO formation in the heterogeneous NO_2 hydrolysis reaction itself. Such a photoenhancement of the fundamental heterogeneous hydrolysis is reasonable in light of the proposed mechanism shown in Fig. 1. For example, conversion of symmetric N_2O_4 to asymmetric N_2O_4 in a methylcyclohexane matrix at 77 K has been reported during photolysis at 313 and 365 nm,[32] which would increase the rate of formation of HONO (see Fig. 1). Such a photoenhancement is also consistent with reports from field studies of significant daytime sources of HONO.[10,33,34]

Recently Zhou *et al.*[33,35,36] reported evidence for a photochemical production of HONO from HNO_3 deposited on surfaces. This HONO production was first observed in a glass sampling line exposed to sunlight during a field study,[35] and was confirmed in subsequent laboratory experiments.[36] The mechanism proposed by Zhou and coworkers involves photolysis of nitric acid *via* two reaction channels, one producing HONO + $O(^3P)$ and the other producing NO_2 + OH, followed by a photoenhanced version of reaction (1) as reported by Akimoto *et al.*[1] The analytical technique used in these experiments involves uptake of HONO into solution and

DOI: 10.1039/b402195a

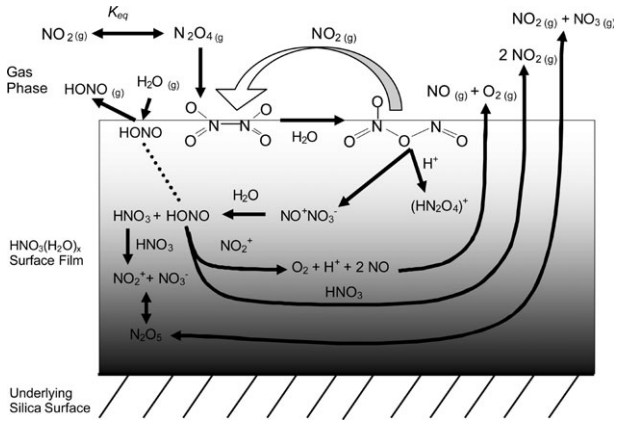

Fig. 1 Schematic of the reaction mechanism of the heterogeneous hydrolysis of NO_2 proposed by Finlayson-Pitts *et al.*[12] with the inclusion of competitive adsorption between water and HONO.[30]

measurement as nitrite by reaction with sulfanilamide and *N*-(1-naphthyl)-ethylenediamine to form a strong, light-absorbing azo dye; this is separated and analyzed using HPLC with an absorption detector. The sensitivity for HONO is 5 ppt or better. While no significant artifacts have been reported using this method, in principle any species that forms nitrite in solution will give a positive response. Given the number of potential surface products and intermediates involved in heterogeneous NO_x chemistry (Fig. 1), the possible contribution of other compounds in the HONO measurement cannot be dismissed with certainty.

In short, understanding the photolytic sources of HONO is not only of fundamental chemical interest, but is also key for understanding field measurements of HONO and for accurate modeling of urban airsheds. In addition, it is critical for interpreting the data from environmental chambers where a substantial flux of HONO has been observed from the chamber walls during photolysis.[37–42]

In the present study, HONO formation from NO_2 hydrolysis in a borosilicate glass cell has been studied in the presence and absence of UV radiation (320–400 nm). The data are interpreted in the framework of a simplified mechanism similar to that shown in Fig. 1, along with a kinetics model developed to describe the reaction in the absence and presence of radiation. A comparison of the experimental data to the model predictions clearly establishes that while there is no photoenhancement in the kinetics of the NO_2 hydrolysis itself, photolysis of surface-adsorbed HNO_3 from this reaction does indeed act as a HONO source as proposed by Zhou *et al.*[33,35,36] Because HONO is measured directly in the present study, any uncertainties regarding potential contributions of species other than HONO are removed. Insights from earlier studies of heterogeneous NO_x chemistry in this laboratory are used to propose a mechanism involved in the photolysis of surface-adsorbed HNO_3 to generate gas phase HONO and NO_2. The implications for environmental chamber studies and for chemistry in the polluted troposphere are discussed.

Experimental methods

A. Experimental

A cylindrical borosilicate glass long path cell (0.15 m id, 1 m base path, 19.4 L volume, and a ratio of the surface (including optics[12]) to volume of 46 m^{-1} was used as a reaction vessel. The cell was equipped with a set of White optics[43] aligned for a path length of 84 m. The flanges and inner supports consist of anodized aluminum covered with a thin coating of halocarbon wax (Halocarbon Products, Inc., Series 1500) to avoid reactions with metal surfaces. Ultraviolet radiation (320–400 nm) entered the cell through the glass walls from a single 0.9 m long blacklamp (Sylvania, 30 W, F30T8/350BL) aligned vertically along the side of the cell, irradiating the entire cell and its contents.

Concentrations of NO_2, HONO, and NO in the cell were measured using FTIR (Mattson, Research Series). Spectra were typically collected at a resolution of 1 cm^{-1} and consisted of 16–64 co-added scans collected over 18–51 s. Gas phase NO_2, HONO, and NO were quantified by the net absorbance of their peaks at 2917, 1263, and 1875 cm^{-1}, respectively. Concentrations of NO_2 and NO were determined based on calibrations using mixtures of known concentrations in N_2 in the cell. The HONO concentrations were calculated using the 1263 cm^{-1} peak due to the *trans*-isomer and applying an effective absorption cross section of $(3.7 \pm 0.4) \times 10^{-19}$ cm^2 $molecule^{-1}$ (base 10) to measure total HONO based on a *trans*/*cis* ratio of 2.3.[44] Concentrations of H_2O were determined by flowing a known concentration of water vapor through the cell and measuring rotational lines at 1174 cm^{-1} and 1187 cm^{-1}.

In each NO_2 hydrolysis experiment, ~20–50 ppm NO_2 were introduced to the cell as a mixture in nitrogen or air. The cell was then filled to atmospheric pressure by opening it to a collapsible Teflon chamber that contained humid N_2 or air obtained by flowing the carrier gas through a bubbler containing water and mixing it with dry carrier gas. This method quickly brought the cell pressure to 1 atm at the desired relative humidity (RH). Nitrous acid accumulated for 2–3 h *via* the hydrolysis of NO_2 before irradiation began. Photolysis periods typically lasted for 2–3 h. All experiments were performed at 296 ± 1 K.

In order to model the system quantitatively, the photolysis rate constants for NO_2 and HONO in this system were acquired. For NO_2, this was determined experimentally by adding NO_2 to the cell in concentrations similar to those in the hydrolysis experiments. The cell was filled to 1 atm with N_2, irradiated and the decay of NO_2 measured. The NO_2 photolysis rate constant was calculated using the method of Holmes *et al.*,[45] based on the following mechanism, reactions (H1)–(H7) (see Table 1 for rate constants):

$$NO_2 + h\nu \xrightarrow{k_p^{NO_2}} NO + O \qquad (H1)$$

$$O + NO_2 \xrightarrow{k_{H2}} NO + O_2 \qquad (H2)$$

$$O + NO_2 + M \xrightarrow{k_{H3}} NO_3 + M \qquad (H3)$$

$$O + NO + M \xrightarrow{k_{H4}} NO_2 + M \qquad (H4)$$

$$NO_3 + NO \xrightarrow{k_{H5}} 2NO_2 \qquad (H5)$$

$$NO_3 + NO_2 + M \xleftrightarrow{k_{H6}} N_2O_5 + M \qquad (H6)$$

$$NO_3 + NO_2 \xrightarrow{k_{H7}} NO + NO_2 + O_2 \qquad (H7)$$

With the appropriate steady state assumptions for NO, NO_3, and N_2O_5 in an O_2 deficient environment, the photolysis rate constant for NO_2 ($k_p^{NO_2}$) was determined using the following relationship:[45]

$$k_p^{NO_2} = \frac{Z}{2t} \qquad (I)$$

where t is time and Z is given by eqn. (II):

$$Z = \left\{ \left(1 + \frac{k_{H3}[M]}{k_{H2}} - \frac{k_{H4}[M]}{k_{H2}}\right)\left(\ln\frac{[NO_2]_0}{[NO_2]}\right) + \left(\frac{k_{H4}[M]}{k_{H2}}\right)\left(\frac{[NO_2]_0}{[NO_2]} - 1\right)\right\} \qquad (II)$$

Table 1 Chemical reactions in model

Reaction		Rate constant (k^{298})[a]	Reference
A. Gas phase reactions			
$2NO_2 \xrightarrow{M} N_2O_4$		2.5×10^{-14}	Atkinson *et al.*, 2002
$N_2O_4 \rightarrow 2\ NO_2$		1.1×10^{5}	Atkinson *et al.*, 2002
$NO_3+NO \rightarrow 2\ NO_2$		2.6×10^{-11}	Sander *et al.*, 2003
$NO_2+NO_3 \xrightarrow{M} N_2O_5$		1.2×10^{-12}	Sander *et al.*, 2003
$N_2O_5 \rightarrow NO_2+NO_3$		3.8×10^{-2}	Sander *et al.*, 2003
$NO_2+O(^3P) \rightarrow NO+O_2$		1.0×10^{-11}	Sander *et al.*, 2003
$NO_2 + O(^3P) \xrightarrow{M} NO_3$		3.3×10^{-12}	Sander *et al.*, 2003
$NO_2+O_3 \rightarrow NO_3+O_2$		3.2×10^{-17}	Sander *et al.*, 2003
$NO_2 + OH \xrightarrow{M} HNO_3$		1.0×10^{-11}	Sander *et al.*, 2003
$NO_2+OH \xrightarrow{M} HOONO$		2.1×10^{-12}	Sander *et al.*, 2003
$HOONO \rightarrow NO_2 + OH$		1.1	Sander *et al.*, 2003
$NO_2 + HO_2 \xrightarrow{M} HO_2NO_2$		1.4×10^{-12}	Sander *et al.*, 2003
$HO_2NO_2 \rightarrow NO_2 + HO_2$		8.6×10^{-2}	Sander *et al.*, 2003
$NO + NO_2 \xrightarrow{M} N_2O_3$		7.2×10^{-15}	Atkinson *et al.*, 2002
$N_2O_3 \rightarrow NO + NO_2$		3.8×10^{5}	Atkinson *et al.*, 2002
$NO + O(^3P) \xrightarrow{M} NO_2$		1.7×10^{-12}	Sander *et al.*, 2003
$2\ NO + O_2 \rightarrow 2\ NO_2$		2.0×10^{-38}	Atkinson *et al.*, 2002
$NO + O_3 \rightarrow NO_2 + O_2$		1.9×10^{-14}	Sander *et al.*, 2003
$NO + OH \xrightarrow{M} HONO$		7.4×10^{-12}	Sander *et al.*, 2003
$NO + HO_2 \rightarrow OH + NO_2$		8.1×10^{-12}	Sander *et al.*, 2003
$NO_3 + O(^3P) \rightarrow O_2 + NO_2$		1.0×10^{-11}	Sander *et al.*, 2003
$NO_3 + OH \rightarrow HO_2 + NO_2$		2.2×10^{-11}	Sander *et al.*, 2003
$NO_3 + HO_2 \rightarrow OH + NO_2 + O_2$		3.5×10^{-12}	Sander *et al.*, 2003
$N_2O + O(^1D) \rightarrow N_2 + O_2$		4.9×10^{-11}	Sander *et al.*, 2003
$O(^1D) + O_2 \rightarrow O(^3P) + O_2$		4.0×10^{-11}	Sander *et al.*, 2003
$HONO + OH \rightarrow H_2O + NO_2$		4.5×10^{-12}	Sander *et al.*, 2003
$HONO + O(^3P) \rightarrow NO_2 + OH$		9.1×10^{-16}	Tsang and Herron, 1991
$N_2O + O(^1D) \rightarrow 2\ NO$		6.7×10^{-11}	Sander *et al.*, 2003
$O(^3P) + O_2 \xrightarrow{M} O_3$		1.5×10^{-14}	Sander *et al.*, 2003
$O(^1D) + O_3 \rightarrow 2\ O_2$		1.2×10^{-10}	Sander *et al.*, 2003
$O(^1D) + O_3 \rightarrow 2\ O(^3P) + O_2$		1.2×10^{-10}	Sander *et al.*, 2003
$O(^3P) + O_3 \rightarrow 2\ O_2$		8.0×10^{-15}	Sander *et al.*, 2003
$H + O_2 \xrightarrow{M} HO_2$		1.2×10^{-12}	Sander *et al.*, 2003
$O(^1D) + H_2O \rightarrow 2\ OH$		2.2×10^{-10}	Sander *et al.*, 2003
$O(^3P) + H_2O_2 \rightarrow OH + HO_2$		1.7×10^{-15}	Sander *et al.*, 2003
$OH + O_3 \rightarrow HO_2 + O_2$		7.3×10^{-14}	Sander *et al.*, 2003
$2\ OH \rightarrow O(^3P) + H_2O$		1.9×10^{-12}	Sander *et al.*, 2003
$2OH \xrightarrow{M} H_2O_2$		6.3×10^{-12}	Sander *et al.*, 2003
$OH + HO_2 \rightarrow O_2 + H_2O$		1.1×10^{-10}	Sander *et al.*, 2002
$H + O_3 \rightarrow OH + O_2$		2.9×10^{-11}	Sander *et al.*, 2003
$OH + H_2O_2 \rightarrow HO_2 + H_2O$		1.7×10^{-12}	Sander *et al.*, 2003
$HO_2 + O_3 \rightarrow OH + 2\ O_2$		1.9×10^{-15}	Sander *et al.*, 2003
$O(^3P) + OH \rightarrow O_2 + H$		3.3×10^{-11}	Sander *et al.*, 2003
$O(^3P) + HO_2 \rightarrow OH + O_2$		5.9×10^{-11}	Sander *et al.*, 2003
$OH + HNO_3 \rightarrow H_2O + NO_3$		1.5×10^{-13}	Sander *et al.*, 2003
$2\ HO_2 \rightarrow H_2O_2 + O_2$	0%RH	2.9×10^{-12}	Sander *et al.*, 2003
	50%RH	5.4×10^{-12}	Sander *et al.*, 2003
	80%RH	6.9×10^{-12}	Sander *et al.*, 2003
$NO_2 + H \rightarrow OH + NO$		1.3×10^{-10}	Sander *et al.*, 2003
B. Photolysis reactions			
$NO_2 \xrightarrow{h\nu} NO + O(^3P)$		$(1.7 \pm 0.1) \times 10^{-3}$	Measured[b]
$HONO \xrightarrow{h\nu} NO + OH$		$(4.9 \pm 1.4) \times 10^{-4}$	Measured[c]
$HONO_{(ads)} \xrightarrow{h\nu} NO + OH$		$(4.9 \pm 1.4) \times 10^{-4}$	Estimated
$O_3 \xrightarrow{h\nu} O_2 + O(^1D)$		$(4.7 \pm 0.1) \times 10^{-5}$	Calculated[d]
C. Surface reactions			
$NO_{2(g)} + H_2O_{(g)} \rightarrow HONO_{(ads)}$		$(2.4 \pm 0.4) \times 10^{-23}$	Model fit[e]
$NO_{2(g)} + H_2O_{(g)} \rightarrow HNO_{3(ads)}$		$(2.4 \pm 0.4) \times 10^{-23}$	Model fit[e]
$HONO_{(ads)} + H_2O \rightarrow HONO_{(g)} + H_2O$		1.35×10^{-20}	Model fit
$HONO_{(ads)} \rightarrow NO_{(g)}$		8.0×10^{-4}	Model fit
$HONO_{(g)} \rightarrow HONO_{(ads)}$		2.0×10^{-4}	Measured
$HONO_{(ads)} + HNO_{3(ads)} \rightarrow 2\ NO_2$		1.0×10^{-17}	Model fit
$OH_{(g)} \rightarrow$ wall loss		700	See text[f]
$N_2O_5 \rightarrow 2\ HNO_{3(ads)}$		83	[g]

[a] Termolecular reactions with a third body are accounted for in the rate constants using [M] = 2.46×10^{19} molecules cm^{-3} to match experimental conditions. Rate constants are in the units of cm^3 molecule^{-1} s^{-1} or s^{-1}. [b] Experimentally measured as described in the text. Errors shown are 2*s*. [c] Experimentally measured in the cell using cyclohexane as an OH scavenger. Errors shown are 2*s*. [d] Calculated using an analogue of eqn. (IV). [e] The rates of these reactions were always taken as being equal; by expressing the production of HONO and HNO_3 separately, the first order kinetics in NO_2 and H_2O was captured. [f] Equivalent to a reaction probability for wall loss of OH of 0.1.[67] [g] Equivalent to a reaction probability of 0.03.[68]

In eqn. (II), $[NO_2]_0$ is the initial NO_2 concentration, $[NO_2]$ is the concentration at time t, k_{H2}, k_{H3}, and k_{H4} are the rate constants for reactions (H2), (H3), and (H4) respectively, and M is the required third body, in this case N_2. The NO_2 photolysis rate constant was obtained from the slope of a plot of Z versus time. From data such as those shown in Fig 2, the NO_2 photolysis rate constant ($k_p^{NO_2}$) was determined to be $(1.7 \pm 0.1) \times 10^{-3}$ s^{-1} (2s).

To determine the HONO photolysis rate constant, 100–200 ppm of cyclohexane was added to mixtures of HONO (0.2–1.8 ppm) in N_2 in order to scavenge the OH and prevent the regeneration of HONO from the OH + NO recombination reaction and the loss of HONO from secondary reactions, such as HONO + OH. The HONO decay was treated as first order and the HONO photolysis rate constant was obtained from eqn. (III):

$$\ln\frac{[\mathrm{HONO}]_0}{[\mathrm{HONO}]} = k_p^{\mathrm{HONO}} t \qquad \text{(III)}$$

The photolysis rate constant for HONO (k_p^{HONO}) was determined from data such as those shown in Fig 3 to be $(4.9 \pm 1.4) \times 10^{-4}$ s^{-1} (2s). As a further check on the experimentally determined HONO photolysis rate constant, eqn. (IV) was also used to calculate k_p^{HONO} based on the measured value of $k_p^{NO_2}$:

$$\frac{k_p^{\mathrm{HONO}}}{k_p^{\mathrm{NO_2}}} = \frac{\int_{320\ \mathrm{nm}}^{400\ \mathrm{nm}} \Phi_{\mathrm{HONO}}(\lambda)\sigma_{\mathrm{HONO}}(\lambda)F(\lambda)\,\mathrm{d}\lambda}{\int_{320\ \mathrm{nm}}^{400\ \mathrm{nm}} \Phi_{\mathrm{NO_2}}(\lambda)\sigma_{\mathrm{NO_2}}(\lambda)F(\lambda)\,\mathrm{d}\lambda} \qquad \text{(IV)}$$

In eqn. (IV), σ is the relevant base e absorption cross section,[46,52] Φ is the corresponding quantum yield, and $F(\lambda)$ is the wavelength-dependent intensity of light. The values of $F(\lambda)$ are given by $I(\lambda)$ C, where $I(\lambda)$ is obtained from the manufacturer supplied spectral light distribution and C is a constant that takes into account the overall light intensity for this experimental configuration. The constant C cancels out so that the spectral distribution $I(\lambda)$ can be substituted for $F(\lambda)$ in eqn. (IV). This calculation yielded a value of $k_p^{HONO} = (5.0 \pm 1.5) \times 10^{-4}$ s^{-1} (2s), in excellent agreement with the measured value of $(4.9 \pm 1.4) \times 10^{-4}$ s^{-1}. This agreement establishes that additional sources of HONO such as NO_2 heterogeneous hydrolysis and HNO_3 photolysis (see below) are not significant under the conditions under which k_p^{HONO} was measured.

B. Materials

Nitric oxide (Matheson, 99%) was purified by passing it through a liquid nitrogen trap to remove impurities such as NO_2 and HNO_3. Nitrogen dioxide was synthesized by reacting the purified NO with excess oxygen (Oxygen Service Company, 99.993%) for at least 2 h. The NO_2 was then purified by condensing in a cold finger at 195 K and pumping away the excess O_2.

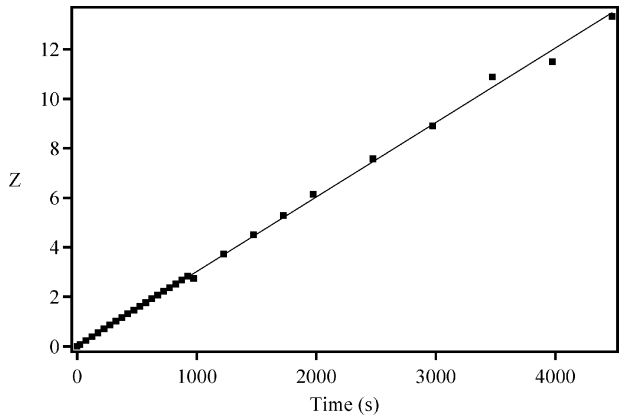

Fig. 2 Typical data for the loss of NO_2 during photolysis plotted in the form of eqn. (I) (see text).

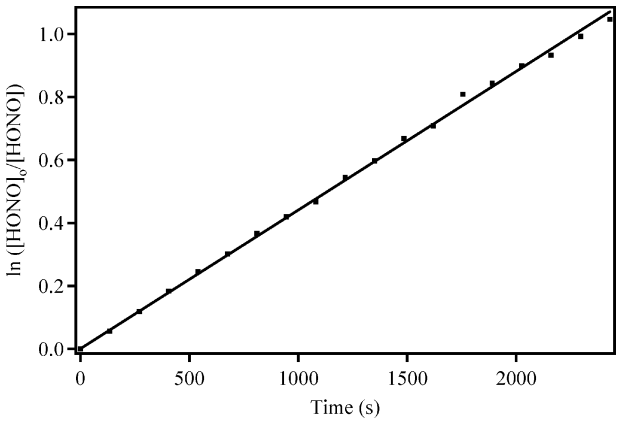

Fig. 3 Typical first order plot for the photolysis of 1.2 ppm HONO in the presence of 135 ppm of cyclohexane.

Nitrous acid was synthesized by reacting HCl with $NaNO_2$:

$$NaNO_2 + HCl \longrightarrow HONO + NaCl$$

Solid $NaNO_2$ (Aldrich, 99.5%) was exposed to humid N_2 (80-100% RH) for 15–20 minutes to moisten the salt surface. The flow of humid N_2 was stopped and replaced with a flow of gaseous HCl prepared by passing dry N_2 over a HCl solution (Fisher, Certified ACS Plus, 12.1 M diluted ~1:3 (v:v) using Nanopure® water).

The nitrogen (Oxygen Service Company, 99.999%), air (Oxygen Service Company, <0.1 ppm total hydrocarbons, <0.5 ppm CO, <2.0 ppm H_2O, <0.5 ppm CO_2) and cyclohexane (Fisher, 99.9%) were used as received. The water was Nanopure® ASTM type I reagent grade water (Barnstead, 18.2 MΩ cm).

C. Modeling

A kinetics modeling program (REACT for Windows v.1.2)[47–49] was used to simulate the gas phase chemistry and photolysis as well as the hydrolysis of NO_2 in the cell. The program numerically integrates the differential rate equations representing the reaction kinetics. The model for the dark period includes the gas phase reactions given in section A of Table 1 and the surface chemistry summarized in section C. The model includes the relevant gas phase reactions and kinetics from available databases.[50–52] To represent the chemistry during irradiation, the photolysis reactions listed in section B of Table 1 were included; these are discussed in more detail below. The surface reactions were parameterized as gas phase processes. Because the specific details of the NO_2 heterogeneous hydrolysis mechanism are uncertain, this portion of the model is simplified to have the least number of unknown variables and yet still capture the essence of what is known about the heterogeneous hydrolysis of NO_2: the reaction is first order in NO_2 and water vapor,[12,17–26] there is a competitive adsorption on the surface between H_2O and HONO,[30] and HONO undergoes heterogeneous reactions on the cell walls to generate NO and NO_2.[30,53–59] A more complex mechanism involving N_2O_4 can also be used but since the rate constants for the individual steps are not known, it does not add to the data interpretation during photolysis and hence we have chosen to use this more simplified mechanism in this case.

Rate constants for the surface reactions were adjusted within the constraints of the mechanism to provide a best fit to the observed decay of NO_2 and the formation of HONO during the dark period. By accurately predicting the chemistry in the dark and having measured the photolysis rate constants for NO_2 and HONO, the chemistry should be predicted during the

irradiation period as well if there is no unknown chemistry occurring. The rate constant for the NO_2 heterogeneous hydrolysis was allowed to vary slightly from experiment to experiment to give the best fit to the data in the dark portion of the experiment; a value of $(2.4 \pm 0.4) \times 10^{-23}$ (Table 1) encompassed all of the experiments. This gives accurate initial concentrations for NO_2 and HONO at the end of the dark period. Once the data for a particular experiment were matched for region I, the same rate constants were used during irradiation.The photolysis period was modeled by including the photodissociation of NO_2, HONO, and O_3 in the model (section B of Table 1), along with the chemistry in sections A and C of Table 1.

Results and discussion

Fig 4 shows a typical concentration–time profile for the gaseous reactants and products for the reaction of 46 ppm NO_2 at 39% RH in 1 atm of N_2. In the dark period (region I), the NO_2 concentration slowly decays while HONO increases; NO is initially below the detection limit of 1×10^{13} cm^{-3} and is barely detectable at the end of the dark period. The relatively high detection limit for NO in the presence of water vapor is largely due to the strong overlapping rotational lines of water which need to be subracted from the spectra; in addition, NO is a relatively weak absorber and the concentration-absorbance relationship is non-linear at this resolution. While nitrous acid is the initial product of reaction (1), subsequent reactions of HONO on the surface generate NO and NO_2.[30,53–59] At ~6500 s, the contents of the cell were irradiated (region II). As expected from the large absorption cross sections and quantum yields for NO_2 and HONO in the 300–400 nm region,[11] the concentrations of both compounds decrease. Nitric oxide, the primary photolysis product of these reactions, rapidly increases. After ~650 s of photolysis (region III), the HONO concentration begins to level off while less than 25% of the initial NO_2 remains.

Fig 5 shows expanded plots for the concentration–time profiles for three NO_2 hydrolysis experiments at different relative humidities and initial concentrations of NO_2. The time is referenced to the irradiation period with zero designated as the start of irradiation. In the dark period, there is excellent agreement between the measured concentrations (symbols) and those predicted by the model (solid lines). During the first ~10 min of photolysis (region II), the measured and modeled HONO concentrations agree to within 2% at all times without including any photoenhancement of the NO_2 heterogeneous hydrolysis reaction. This agreement is quite satisfactory, given the simplified mechanism used to treat the surface reactions. The model does not match the NO concentrations quite as well as HONO in region II, but the predicted concentrations are still within the measured error bars for NO.

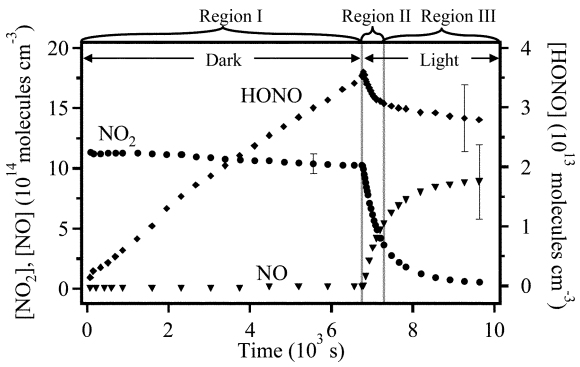

Fig. 4 Experimental concentration–time profiles for NO_2 (●), HONO (◆), and NO (▼) with 46 ppm initial [NO_2] and 39% RH in 1 atm N_2 at 296 K. Typical error bars shown are ± 2s.

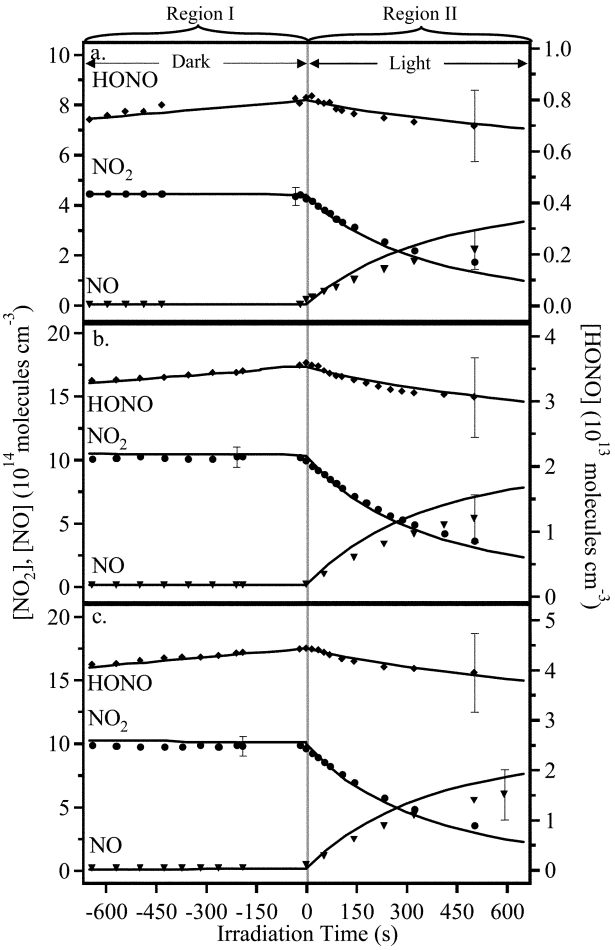

Fig. 5 Comparison of experimental data (symbols) and model-predicted (solid lines) concentration–time profiles for NO_2 (●), HONO (◆), and NO (▼) with (a) 20 ppm initial [NO_2] and 33% RH in N_2 (b) 46 ppm initial [NO_2] and 39% RH in N_2 (c) and 54 ppm initial [NO_2] and 57% RH in N_2. Typical error bars shown are ± 2s.

Fig 6 shows expanded plots of regions II and III for three typical experiments. In region III, the model underestimates the HONO concentrations. Although the 2*s* error bars on the HONO concentrations (which are due primarily to the uncertainty in the measured IR absorption cross section at 1263 cm^{-1}) overlap the model predictions in region III, the model provides a good match to the data at shorter photolysis times (region II), suggesting that errors in the HONO measurement are not responsible for the increasing discrepancy between the experiment and model. One factor could be that there is an additional source of HONO at the longer irradiation times but which is not included in the chemistry shown in Table 1.

Indeed, there is experimental evidence from other laboratories for such a photochemical production of HONO. Zhou *et al.*[35] recently reported significant production of gaseous HONO when a glass sampling manifold was exposed to sunlight and hypothesized that photolysis of HNO_3 on the surface was the source of the additional HONO. In a later laboratory experiment,[36] significant HONO and NO_2 production were observed when 0–80% RH air was irradiated with a filtered mercury arc lamp (>290 nm) in a glass flow cell which had been previously conditioned with gaseous HNO_3 and water vapor.

To test for photolysis of surface-adsorbed nitric acid as a possible source of the additional HONO in region (III), reaction (2) was added to the model:

$$HNO_{3(ads)} + h\nu \xrightarrow{k_2} HONO \qquad (2)$$

The value of k_2 was allowed to vary to match the HONO data

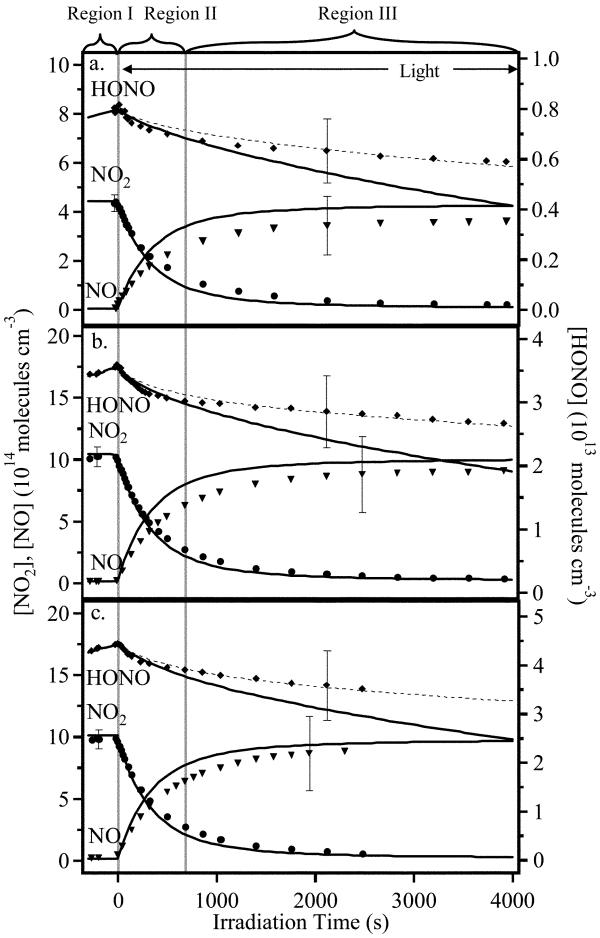

Fig. 6 Comparison of experimental data (symbols), model-predicted (solid lines), and model-predicted with the inclusion of HNO_3 photolysis (dashed lines) concentration–time profiles for NO_2 (●), HONO (◆), and NO (▼) during irradiation with (a) 20 ppm initial [NO_2] and 33% RH in N_2 (b) 46 ppm initial [NO_2] and 39% RH in N_2 (c) and 54 ppm initial [NO_2] and 57% RH in N_2. Typical error bars shown are ± 2s.

in region III. The dotted lines in Fig. 6a–c show the model predictions with $k_2 = 2.1 \times 10^{-5}$, 2.9×10^{-5} and 2.9×10^{-5} s^{-1}, respectively. Including reaction (2) in the model did not change the predicted NO and NO_2 significantly, so that the dotted lines for NO and NO_2 overlay the solid lines. Addition of this photolytic source of HONO provides a much better prediction of the HONO concentrations and is consistent with the proposal of Zhou *et al.*[33,35,36] that the photolysis of nitric acid adsorbed on surfaces generates gas phase HONO. In the present set of experiments, however, HONO was detected directly, removing the ambiguity associated with measuring HONO as nitrite in solution.

Recent experiments in this laboratory shed some light on potential mechanisms of the production of HONO and NO_2 from the photolysis of surface-adsorbed HNO_3.[30,31] First, water competes with HONO for surface sites, so that as the water vapor increases, it displaces HONO.[30] In addition, HONO reacts on surfaces that have been preconditioned with HNO_3 to generate NO_2.[30] The mechanism of the latter reaction may involve protonation of HONO to form NO^+ followed by its reaction with NO_3^- to generate N_2O_4 which dissociates to $2NO_2$ (essentially the reverse of the NO_2 heterogeneous hydrolysis); alternatively, one can envision this reaction occurring through the formation of a hydrogen-bonded complex between HONO and HNO_3 on the surface. A third relevant observation is that nitric acid forms complexes with water on surfaces; indeed, these complexes were first observed in the heterogeneous hydrolysis of NO_2 on high surface area porous glass.[31]

Thus, the $HNO_{3(ads)}$ formed during the reaction will likely be complexed to water on the borosilicate glass surface through hydrogen bonding.[60–64] Photolysis of this complex in the gas phase to generate HONO and H_2O_2 is energetically possible with wavelengths of light below ~710 nm:

$$HNO_3 \cdot H_2O_{(ads)} + h\nu(\lambda < 710\ \text{nm}) \rightarrow HONO_{(ads)} + H_2O_{2(ads)} \quad (3)$$

On a surface, the fate of the adsorbed HONO will be determined in large part by the water vapor concentration which releases HONO to the gas phase through a competitive adsorption process:

$$HONO_{(ads)} + H_2O \rightarrow HONO_{(g)} + H_2O_{(ads)} \quad (4)$$

As the RH is lowered, the adsorbed HONO increasingly reacts with other species such as adsorbed nitric acid and/or its complex, forming NO_2 (the reverse of reaction 1):

$$HONO_{(ads)} + HNO_{3(ads)} \rightarrow 2\ NO_2 + H_2O \quad (5)$$

Zhou *et al.*[36] reported that HONO generation in the photolysis required the presence of some water, but that the rate of production of HONO was relatively insensitive to RH between 20 and 80% RH. This is consistent with the data in Fig. 6b,c where a change in the RH from 39 to 57% at similar NO_2 concentrations does not significantly change the best fit value of k_2. Desorption of $HONO_{(ads)}$ to the gas phase will increase as the water vapor increases. If the concentration of the nitric acid–water complex on the surface decreases with increasing RH, the generation of gas phase HONO will be relatively insensitive to RH, as is observed both here and in the studies of Zhou *et al.*[36] Consistent with this hypothesis is the observation in earlier studies that the concentration of the nitric acid–water complex on a borosilicate glass surface decreased with increasing RH.[31]

As the RH is lowered, reaction (5) becomes more important relative to the competitive desorption, reaction (4), and the yield of gas phase NO_2 increases. This is consistent with the decrease in gas phase HONO and increase in NO_2 observed by Zhou and coworkers during an experiment in which the RH was lowered during the photolysis (see Fig. 1 of Zhou *et al.*[36]). Based on studies in this laboratory,[31,65] once nitric acid–water complexes are formed on a surface, they remain adsorbed even after pumping or purging with dry gas for many hours. Thus even after lowering the RH to 0% RH, such complexes will be available on the surface to generate HONO during photolysis; in this case, however, the HONO generated is converted rapidly to NO_2 *via* reaction (5). There may also be a contribution from the decomposition of HNO_3 in the absence of radiation as observed in other studies,[66] generating NO_2 and the nitrate radical, NO_3.

The values of k_2 that provide a best fit to the data in Fig. 6 are sensitive to a number of factors. The first is the amount of the nitric acid–water complex on the wall that is available to form HONO during photolysis. The model predictions assumed that only the nitric acid formed during that experiment was available for HONO formation. However, as discussed above, the nitric acid–water complex remains strongly adsorbed to the surface even after pumping so that there will be some additional amount, which was not possible to quantify, available from previous experiments. This will cause the model to overestimate the value of k_2 needed to fit the data.

The second factor involves the OH and NO concentrations in region II, since the OH–NO recombination is the major source of gas phase HONO in this region. The model slightly overestimates NO, which will lead to an underestimate of k_2. The OH concentration during photolysis is determined primarily by the NO_2 concentration, due to its removal by the NO_2–OH reaction, which competes with loss of OH to the wall. We have assumed a rate constant for OH wall loss that

corresponds to a reaction probability of 0.1 for uptake of OH on the walls. This is reasonable given that the loss of OH on uncoated borosilicate glass surfaces is known from many decades of fast flow discharge system studies of OH reactions to be rapid. On glass coated with reactive organics, soot or alumina, the reaction probabilities for OH are >0.1;[67] given that the surface in our reactor has a number of surface-adsorbed species (Fig. 1) which are potential reactants with OH, a value of 0.1 is reasonable. If the reaction probability for loss of OH to the walls is taken to be zero, the best fit values of k_2 for the experiments shown in Fig. 6a–c become 0.6×10^{-5}, 2.0×10^{-5}, and 2.0×10^{-5} s^{-1}, respectively. As expected, this value is most sensitive to the wall loss of OH at lower NO_2 concentrations (Fig. 6a) where the wall loss is more competitive with the reaction with NO_2.

Because of these factors, the best fit value for k_2 cannot be directly compared with that of Zhou *et al.*[36] However, it is very clear from our data that the present experiments provide clear and compelling evidence for photochemical production of HONO from surface-adsorbed nitric acid, which is likely in the form of a nitric acid–water complex. In addition, the photolysis of this surface complex is faster than expected for gas phase HNO_3 in our system. Based on the known[52] UV absorption cross sections and quantum yields for photolysis of gas phase HNO_3 and NO_2, and our measured photolysis rate constant for NO_2 in this system, we calculate that the photolysis rate constant for gas phase HNO_3 should be 1.4×10^{-7} s^{-1} in the reaction cell. This is about two orders of magnitude slower than the best fit values of the photolysis rate constant k_2 for the surface complex that are needed to predict our measured gas phase HONO.

The earlier studies in which a photoenhancement of the heterogeneous hydrolysis was reported[1] were performed in air using a much larger (6065 L) chamber that was coated with PFA Teflon, with a filtered high pressure Xe lamp as the light source (>290 nm). In order to determine whether the presence of O_2 affects HONO formation during photolysis, back-to-back experiments were performed in N_2 and then in air. No significant differences were observed, indicating that the presence of oxygen does not alter the observations.

The surface reaction mechanism used by Akimoto *et al.*[1] was as follows:

$$NO_2(g) \longrightarrow NO_{2(wall)} \quad (6)$$

$$NO_{2(g)} + H_2O_{(g)} \longrightarrow HONO_{(g)} \quad (7)$$

$$NO_{2(g)} + H_2O_{(g)} \longrightarrow HNO_{3(wall)} \quad (8)$$

$$NO_{2(g)} + H_2O_{(g)} \longrightarrow NO_{(g)} \quad (9)$$

$$N_2O_{5(g)} + H_2O_{(g)} \longrightarrow 2HNO_{3(wall)} \quad (10)$$

This is similar to our mechanism except that we do not include wall uptake of NO_2 because we have not observed it in a dry system. Instead of reaction (9), NO is generated in our mechanism by a heterogeneous reaction of HONO on the surface. Our mechanism also includes desorption of HONO to the gas phase caused by competitive adsorption of water and HONO, and a heterogeneous reaction of HONO with surface-adsorbed HNO_3 to form NO_2. These steps in the mechanism have all been observed in separate studies of the uptake and reaction of HONO on borosilicate glass surfaces.[30–31,65] Wall loss of OH does not appear to be included in their model, but there is a variety of experimental evidence showing this process is important in reaction chambers. Despite these differences, both our data and model are quite similar to those of Akimoto and coworkers.[1] It seems likely, based on the present results, that the source of the additional HONO observed in the experiments of Akimoto *et al.*[1] was photochemical production of HONO from species adsorbed on the cell walls, as we have observed at longer photolysis times.

The nitric acid–water complexes that we propose as the HONO precursor are formed not only on borosilicate glass, but also on other surfaces such as quartz and Teflon.[31] As a result, this chemistry is expected to occur in any system where nitric acid is formed by heterogeneous reactions on surfaces (e.g., the heterogeneous hydrolysis of NO_2 and N_2O_5), or is formed first in the gas phase (e.g. by the OH-NO_2 reaction) and subsequently taken up on surfaces. This explains the long-standing common observation of a "wall source" of HONO and OH during photolysis of mixtures in environmental chambers having different surface composition.[37–42] It also indicates that avoiding HONO production from the walls in such chambers is impossible if they have been exposed to nitric acid and water vapor, including that found in air. However, as discussed by Zhou *et al.*,[36] the same chemistry occurs on surfaces in the atmosphere, providing a daytime HONO source as well as a means of "renoxification" of nitric acid that has previously been deposited out on the surfaces of particles or boundary layer soils, building materials *etc*. It is critical to take this chemistry into account in models of both environmental chamber experiments as well as the chemistry of the polluted troposphere.

Acknowledgements

We are thankful to the California Air Resources Board (Contract No. 00-323) and the National Science Foundation (Grant No. ATM-0097573) for the support of this work. We would also like to thank J. N. Pitts Jr. and L. M. Wingen for many useful discussions.

References

1 H. Akimoto, H. Takagi and F. Sakamaki, *Int. J. Chem. Kinet.*, 1987, **19**, 539.
2 D. Perner and U. Platt, *Geophys. Res. Lett.*, 1979, **6**, 917.
3 U. Platt, D. Perner, G. W. Harris, A. M. Winer and J. N. Pitts Jr., *Nature*, 1980, **285**, 312.
4 A. M. Winer and H. W. Biermann, *Res. Chem. Intermed.*, 1994, **20**, 423.
5 G. Lammel and J. Cape, *Chem. Soc. Rev.*, 1996, **25**, 361.
6 R. M. Harrison, J. D. Peak and G. M. Collins, *J. Geophys. Res. Atmos.*, 1996, **101**, 14429.
7 G. Lammel, *Formation of Nitrous Acid: Parameterization and Comparison with Observations, Report No. 286*, Max-Planck-Institut-für Meteorologie, Hamburg, 1999, pp. pp. 1–36.
8 C. Schiller, S. Locquiao, T. Johnson and G. Harris, *J. Atmos. Chem*, 2001, **40**, 275.
9 J. Stutz, B. Alicke and A. Neftel, *J. Geophys. Res. Atmos.*, 2002, **107**10.1029/2001JD000390.
10 B. Alicke, U. Platt and J. Stutz, *J. Geophys. Res.*, 2002, **107**10.1029/2000JD000075.
11 B. J. Finlayson-Pitts and J. N. Pitts, *Chemistry of the Upper and Lower Atmosphere: Theory, Experiments and Applications*, Academic Press, New York, 2000.
12 B. J. Finlayson-Pitts, L. M. Wingen, A. L. Sumner, D. Syomin and K. A. Ramazan, *Phys. Chem. Chem. Phys.*, 2003, **5**, 223.
13 P. G. Caudle and K. G. Denbigh, *Trans. Faraday Soc.*, 1953, **49**, 39.
14 M. S. Peters and J. L. Holman, *Ind. Eng. Chem.*, 1955, **47**, 2536.
15 R. F. Graham and B. J. Tyler, *J. Chem. Soc., Faraday Trans. 1*, 1972, **68**, 683.
16 C. England and W. Corcoran, *Ind. Eng. Chem.*, 1974, **13**, 373.
17 F. Sakamaki, S. Hatakeyama and H. Akimoto, *Int. J. Chem. Kinet.*, 1983, **15**, 1013.
18 J. N. Pitts, E. Sanhueza, R. Atkinson, W. Carter, A. Winer, W. Harris and C. Plum, *Int. J. Chem. Kinet.*, 1984, **16**, 919.
19 R. Svensson, E. Ljungstrom and O. Lindqvist, *Atmos. Environ.*, 1987, **21**, 1529.
20 M. Jenkin, R. Cox and D. Williams, *Atmos. Environ.*, 1988, **22**, 487.
21 C. Perrino, F. De Santis and A. Febo, *Atmos. Environ.*, 1988, **22**, 1925.

22 A. Febo and C. Perrino, *Atmos. Environ.*, 1991, **25**, 1055.
23 S. Mertes and A. Wahner, *J. Phys. Chem.*, 1995, **99**, 14000.
24 P. Wiesen, J. Kleffmann, R. Kurtenbach and K. Becker, *Faraday Discuss.*, 1995, **100**, 121.
25 R. Harrison and G. Collins, *J. Atmos. Chem.*, 1998, **30**, 397.
26 J. Kleffmann, K. H. Becker and P. Wiesen, *Atmos. Environ.*, 1998, **32**, 2721.
27 A. L. Goodman, G. M. Underwood and V. H. Grassian, *J. Phys. Chem. A*, 1999, **103**, 7217.
28 W. S. Barney and B. J. Finlayson-Pitts, *J. Phys. Chem. A*, 2000, **104**, 171.
29 A. L. Goodman, E. T. Bernard and V. H. Grassian, *J. Phys. Chem. A*, 2001, **105**, 6443.
30 D. A. Syomin and B. J. Finlayson-Pitts, *Phys. Chem. Chem. Phys.*, 2003, **5**, 5236.
31 Y. Dubowski, A. L. Sumner, E. J. Menke, D. J. Gaspar, J. Newberg, R. C. Hoffman, R. M. Penner, J. C. Hemminger and B. J. Finlayson-Pitts, *Phys. Chem. Chem. Phys.*, 2004, **6**10.1039/b404127e.
32 A. K. Vorobev, A. A. Revsina and V. S. Gurman, *Russ. Chem. Bull.*, 1996, **45**, 809.
33 X. Zhou, K. Civerolo, H. Dai, G. Huang, J. Schwab and K. Demerjian, *J. Geophys. Res.*, 2002, **107**10.1029/2001JD0001539.
34 J. Kleffmann, R. Kurtenbach, J. Lörzer, P. Wiesen, N. Kalthoff, B. Vogel and H. Vogel, *Atmos. Environ.*, 2003, **37**, 2949.
35 X. Zhou, Y. He, G. Huang, T. Thornberry, M. Carroll and S. Bertman, *Geophys. Res. Lett.*, 2002, **29**10.1029/2002GL015080.
36 X. L. Zhou, H. L. Gao, Y. He, G. Huang, S. B. Bertman, K. Civerolo and J. Schwab, *Geophys. Res. Lett.*, 2003, **30**, 221710.1029/2003GL018620.
37 W. P. L. Carter, R. Atkinson, A. M. Winer and J. J. N. Pitts, *Int. J. Chem. Kinet.*, 1981, **13**, 735.
38 W. P. L. Carter, R. Atkinson, A. M. Winer and J. J. N. Pitts, *Int. J. Chem. Kinet.*, 1982, **14**, 1071.
39 A. C. Besemer and H. Nieboer, *Atmos. Environ.*, 1985, **19**, 507.
40 W. A. Glasson and A. M. Dunker, *Environ. Sci. Technol.*, 1989, **23**, 970.
41 F. Sakamaki and H. Akimoto, *Int. J. Chem. Kinet.*, 1988, **20**, 111.
42 J. Killus and G. Whitten, *Int. J. Chem. Kinet.*, 1990, **22**, 547.
43 J. U. White, *J. Opt. Soc. Am.*, 1942, **32**, 285.
44 W. S. Barney, L. M. Wingen, M. J. Lakin, T. Brauers, J. Stutz and B. J. Finlayson-Pitts, *J. Phys. Chem. A*, 2000, **104**, 1692; W. S. Barney, L. M. Wingen, M. J. Lakin, T. Brauers, J. Stutz and B. J. Finlayson-Pitts, *J. Phys. Chem. A*, 2001, **105**, 4166.
45 J. R. Holmes, R. J. O'Brien, J. H. Crabtree, T. A. Hecht and J. H. Seinfeld, *Environ. Sci. Technol.*, 1973, **7**, 519.
46 J. Stutz, E. S. Kim, U. Platt, P. Bruno, C. Perrino and A. Febo, *J. Geophys. Res.*, 2000, **105**, 14585.
47 W. Braun, J. Herron and D. Kahaner, *Int. J. Chem. Kinet.*, 1988, **20**, 51.
48 J. W. Bozzelli, *J. Chem. Ed.*, 2000, **77**, 165.
49 M. J. Manka, *REACT for Windows, Version 1.2*. Alchemy Software, Wesley Chapel, FL, 2001.
50 R. Atkinson, D. L. Baulch, R. A. Cox, J. N. Crowley, R. F. Hampson, J. A. Kerr, M. J. Rossi and J. Troe, *IUPAC Subcommittee on Gas Kinetic Data Evaluation for Atmospheric Chemistry*, Chemical Kinetics Data Center, NIST, Gaithersburg, MD, 2002.
51 W. Tsang and J. T. Herron, *J. Phys. Chem. Ref. Data*, 1991, **20**, 609.
52 S. P. Sander, A. R. Ravishankara, R. R. Friedl, D. M. Golden, C. E. Kolb, M. J. Kurylo, M. J. Molina, R. E. Huie, V. L. Orkin, G. K. Moortgat, B. J. Finlayson-Pitts, *"Chemical Kinetics and Photochemical Data for Use in Atmospheric Studies". Evaluation Number 14, Jet Propulsion Laboratory*, California Institute of Technology, Pasadena, CA, 2003.
53 M. E. Jenkin, R. A. Cox and D. J. Williams, *Atmos. Environ.*, 1988, **22**, 487.
54 W. H. Chan, R. J. Nordstrom, J. G. Calvert and J. H. Shaw, *Env. Sci. Technol.*, 1976, **10**, 674.
55 W. H. Chan, R. J. Nordstrom, J. G. Calvert and J. H. Shaw, *Chem. Phys. Lett.*, 1976, **37**, 441.
56 E. W. Kaiser and C. H. Wu, *J. Phys. Chem.*, 1977, **81**, 1701.
57 E. W. Kaiser and C. H. Wu, *J. Phys. Chem.*, 1977, **81**, 187.
58 T. J. Wallington and S. M. Japar, *J. Atmos. Chem.*, 1989, **9**, 399.
59 H. M. Ten Brink and H. Spoelstra, *Atmos. Environ.*, 1998, **32**, 247.
60 F.-M. Tao, K. Higgins, W. Klemperer and D. D. Nelson, *Geophys. Res. Lett.*, 1996, **23**, 1797.
61 M. Staikova and D. J. Donaldson, *Phys. Chem. Chem. Phys.*, 2001, **3**, 1999.
62 P. R. McCurdy, W. P. Hess and S. S. Xantheas, *J. Phys. Chem. A*, 2002, **106**, 7628.
63 R. Escribano, M. Couceiro, P. C. Gómez, E. Carrasco, M. A. Moreno and V. J. Herrero, *J. Phys. Chem. A*, 2003, **107**, 651.
64 D. Fernández, V. Botella, V. J. Herrero and R. Escribano, *J. Phys. Chem.*, 2003, **107**, 10608.
65 K. A. Ramazan, L. M. Wingen and B. J. Finlayson-Pitts, unpublished data, 2004.
66 J. N. Crowley, J. P. Burrows, G. K. Moortgat, G. Poulet and G. LeBras, *Int. J. Chem. Kinet.*, 1993, **25**, 795.
67 A. Bertram, A. V. Ivanov, M. Hunter, L. T. Molina and M. J. Molina, *J. Phys. Chem. A*, 2001, **105**, 9415.
68 J. H. Hu and J. P. D. Abbatt, *J. Phys. Chem. A.*, 1997, **101**, 871.